Electronic Supplementary Information for:

A Lamellar Zn-Based Coordination Polymer Showing Increasing Photoluminescence upon Dehydration

Oier Pajuelo-Corral [1], Jose Angel García [2], Oscar Castillo [3,4], Antonio Luque [3,4], Claudio Mendicute-Fierro [1], Antonio Rodríguez-Diéguez [5] and Javier Cepeda [1,*]

[1] Departamento de Química Aplicada, Facultad de Química, Universidad del País Vasco/Euskal Herriko Unibertsitatea (UPV/EHU), 20018 Donostia, Spain; oier.pajuelo@ehu.eus (O.P.-C.); claudio.mendicute@ehu.eus (C.M.-F.)
[2] Departamento de Física, Facultad de Ciencia y Tecnología, Universidad del País Vasco/Euskal Herriko Unibertsitatea (UPV/EHU), 48940 Leioa, Spain; joseangel.garcia@ehu.eus
[3] Departamento de Química Orgánica e Inorgánica, Facultad de Ciencia y Tecnología, Universidad del País Vasco/Euskal Herriko Unibertsitatea (UPV/EHU), 48940 Leioa, Spain; oscar.castillo@ehu.eus (O.C.); antonio.luque@ehu.eus (A.L.)
[4] BCMaterials, Basque Center for Materials, Applications and Nanostructures, UPV/EHU Science Park, 48940 Leioa, Spain
[5] Departamento de Química Inorgánica, Facultad de Ciencias, Universidad de Granada, 18071 Granada, Spain; antonio5@ugr.es
* Correspondence: javier.cepeda@ehu.es; Tel.: +34-943015409

Contents:

S1. Structural details.

S2. Continuous Shape Measurements (CShMs).

S3. Powder X-ray Diffraction Analysis.

S4. Study of the dehydration reversibility of compound **1**$_{an}$.

S5. FT-IR spectroscopy.

S6. Photoluminescence measurements and calculations.

S1. Additional structural details.

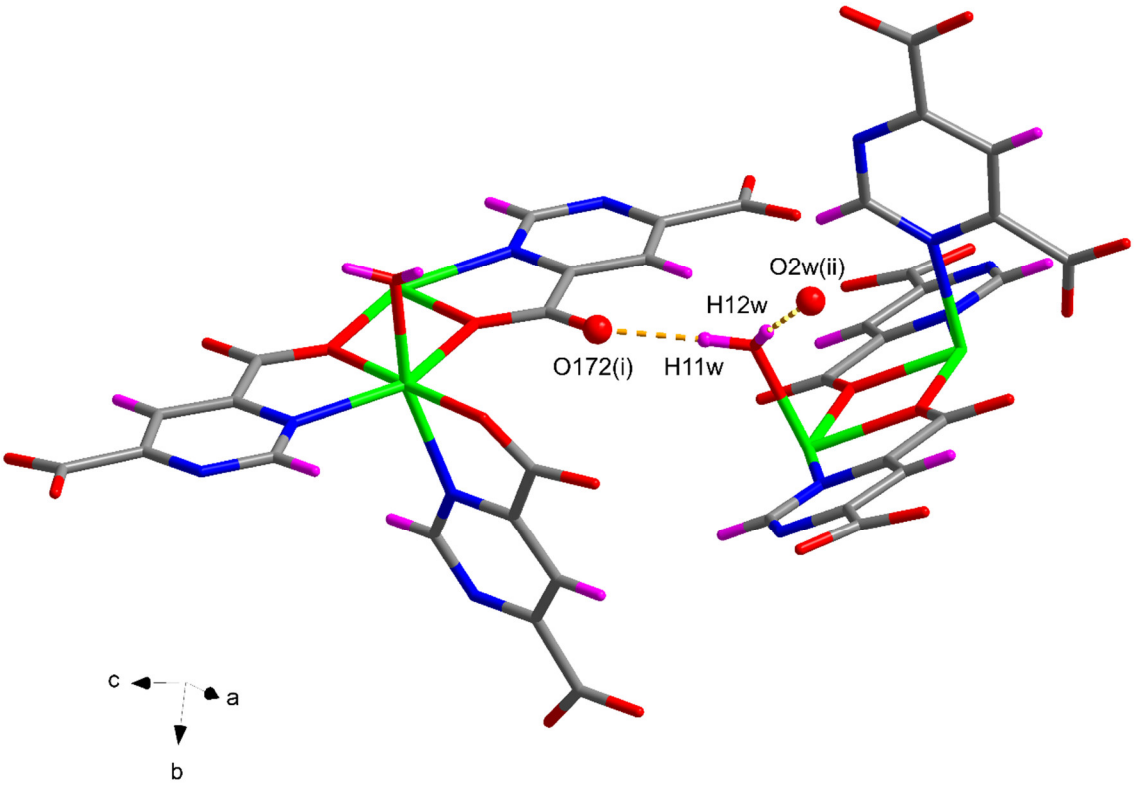

Figure S1. Representation of the C ligand bonds.

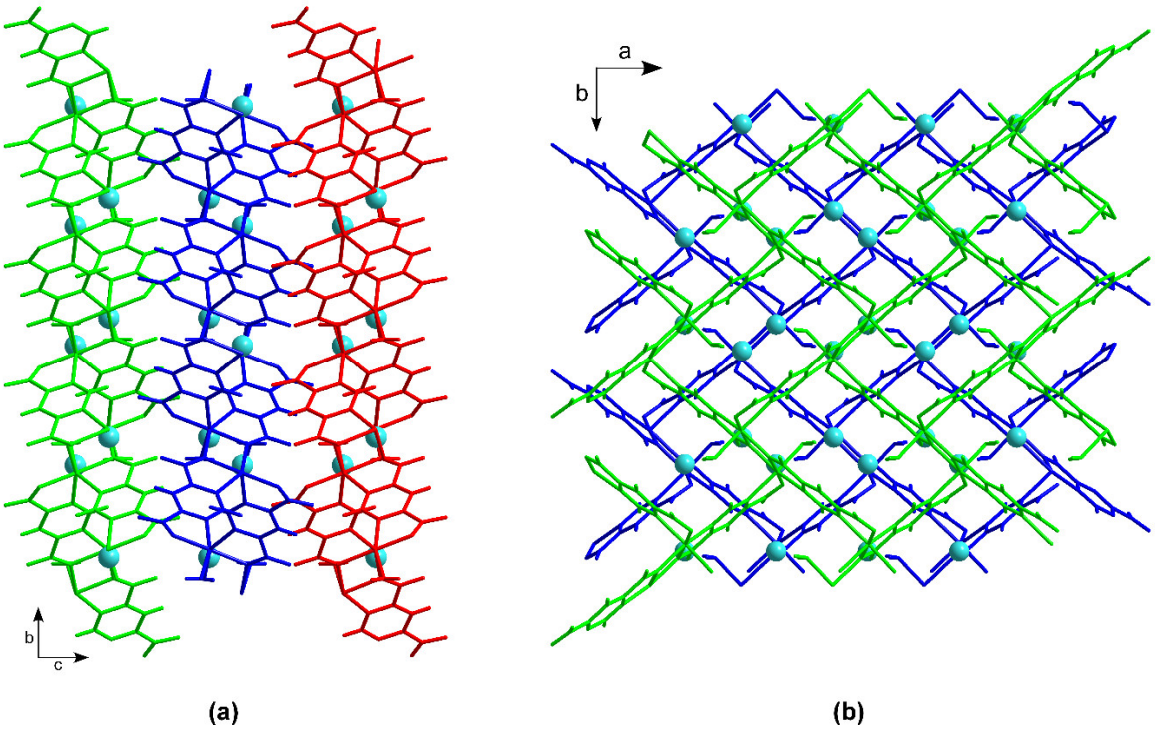

Figure S2. Packing of compound 1 along the (a) *a* axis and (b) *c* axis viewing directions.

Table S1. Hydrogen bonding interactions (Å, °) of compound **1**.[a]

D–H···A[b]	*D–H*	*H···A*	*D···A*	*D–H···A*
O1w–H11w···O172(i)	0.86	1.87	2.725(4)	177.5
O1w–H12w···O2w(ii)	0.86	1.84	2.693(5)	169.3

[a] Symmetry codes: (i) –x + 3/2, –y + 1, z + 1/2; (ii) –x + 1, –y + 1, –z. [b] D: donor. A: acceptor.

S2. Continuous Shape Measurements (CShMs).

Table S2. Continuous Shape Measurements for the coordination environment for compounds **1**. The lowest SHAPE values is shown in bold blue, indicating best fits.

Codes:

HP-6 1 D6h Hexagon

PPY-6 2 C5v Pentagonal pyramid

OC-6 3 Oh Octahedron

TPR-6 4 D3h Trigonal prism

JPPY-6 5 C5v Johnson pentagonal pyramid J2

Structure [ML6]	**HP-6**	**PPY-6**	**OC-6**	**TPR-6**	**JPPY-6**
Comp 1-Zn1	32.557	21.916	**2.907**	11.294	25.502

S3. Powder X-ray Diffraction Analysis.

As observed in Figure S3, the diffraction pattern acquired on the polycrystalline sample obtained by solvent-free procedure fits perfectly the unit cell parameters (and calculated Bragg positions) of the single-crystal data, which confirms the purity of the sample.

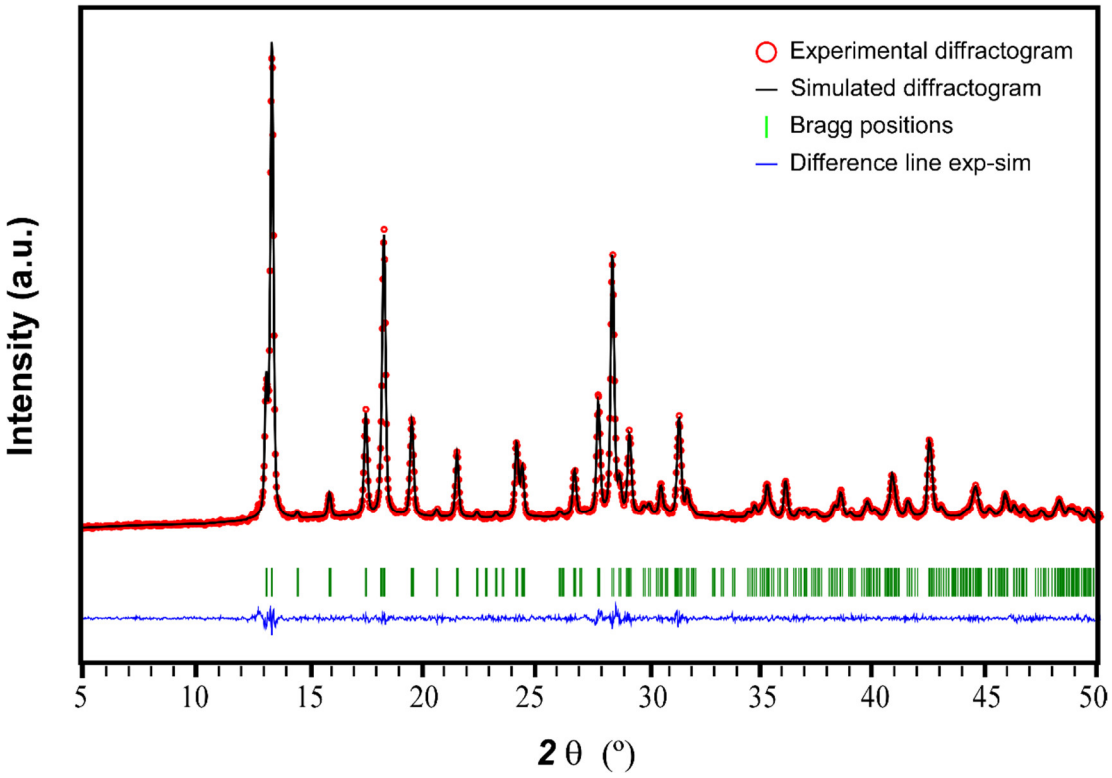

Figure S3. Pattern-matching analysis of polycrystalline sample of compound **1**.

S4. Study of the dehydration reversibility of compound $\mathbf{1}_{an}$.

With the aim of checking if the completely anhydrous compound $\mathbf{1}_{an}$ can revert back to compound **1** by means of a water adsorption process, we carried out a simple experiment in which the sample of $\mathbf{1}_{an}$ was exposed to water vapor. For the experiment, we placed the sample in a small glass vial and, in turn, we placed the vial into a bigger vessel containing distilled water. The vials were left at in a sand-bath at 50 ºC for 5 days, in such a way that water vapor was gently generated. Finally, the vials were open, the sample recovered and analyzed by PXRD technique, by which a similar pattern to the initial amorphous compound was obtained.

Figure S4. Photograph showing the exposure of sample of compound $\mathbf{1}_{an}$ to water vapours. The sample is contained in a vial which, in turn, is placed inside a bigger vial containing water.

S5. FT-IR spectroscopy.

Infrared spectroscopy was used as an initial characterization technique to check the presence of pmdc in compound **1** (Figure S4). The spectrum shows a wide band in the 3550-3100 cm^{-1} which can be assigned to the characteristic band of OH vibrations of water molecules and to the C-H vibration of the pyrimidinic ring of pmdc. The intense peaks that appear at approximately 1650 and 1360 cm^{-1} correspond to the asymmetric and symmetric stretching vibration of the carboxylate groups. In the 1300-1000cm^{-1} region several medium- and weak-intensity peaks appear that can be attributed to the distortions originated in the aromatic ring of pmdc ligand. The bands appearing below 550 cm^{-1} are originated from the M-O and M-N bonds. A comparison of the FTIR spectrum with that of the free ligand can be found in Figure S5.

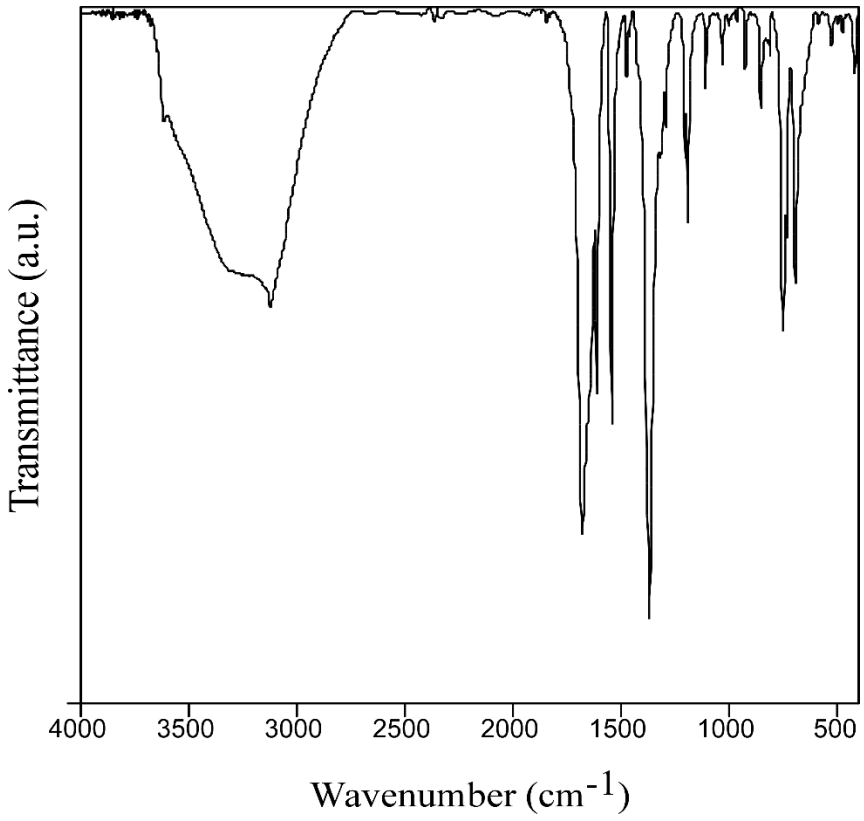

Figure S5. FTIR spectrum of compound **1**.

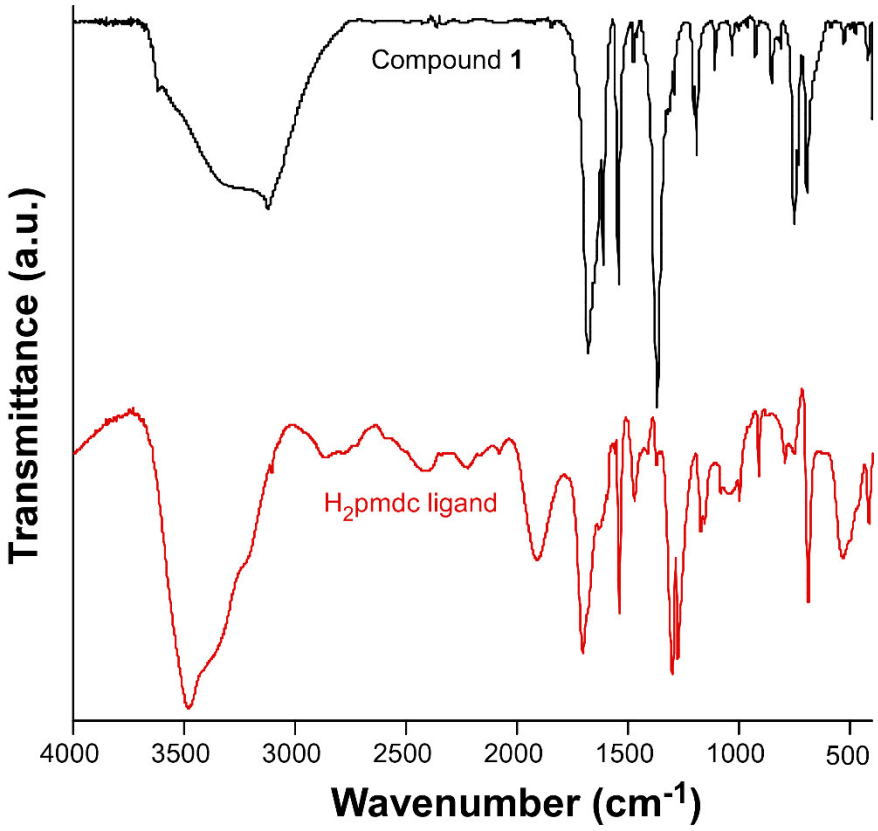

Figure S6. Comparison of the FTIR spectra of compound **1** and the free H_2pmdc ligand.

S6. Photoluminescence measurements and calculations.

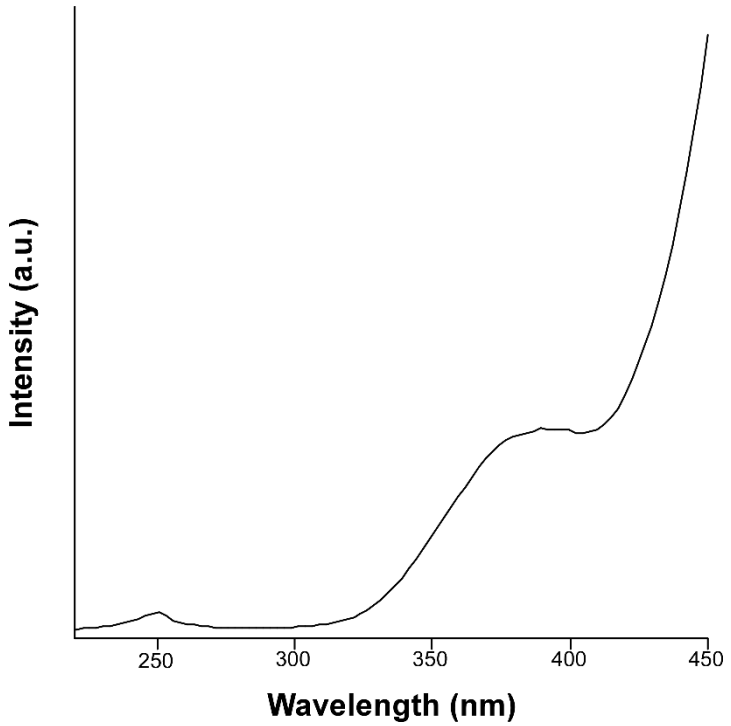

Figure S7. Excitation spectrum of compound **1** taken at room temperature at λ_{em} = 495 nm.

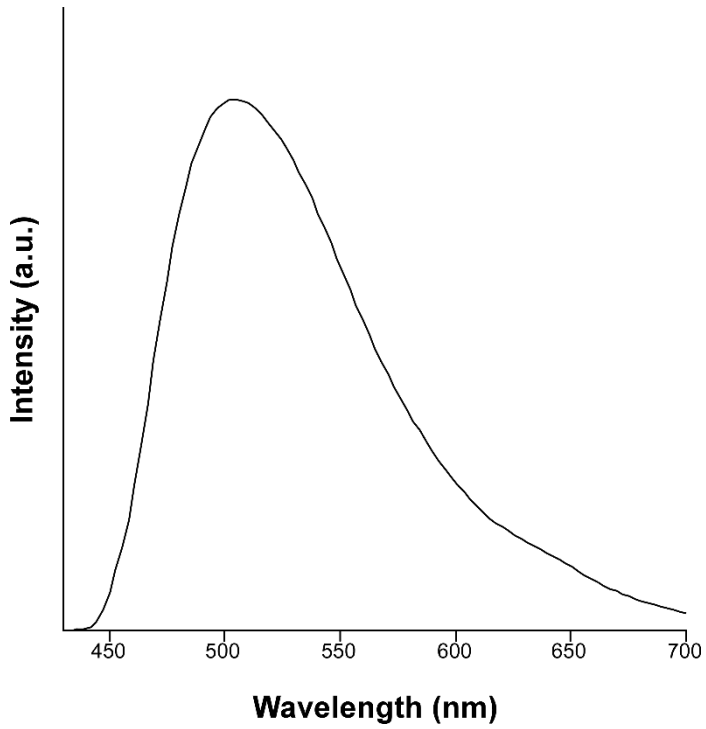

Figure S8. Emission spectrum of compound **1** measured at room temperature at λ_{em} = 375 nm.

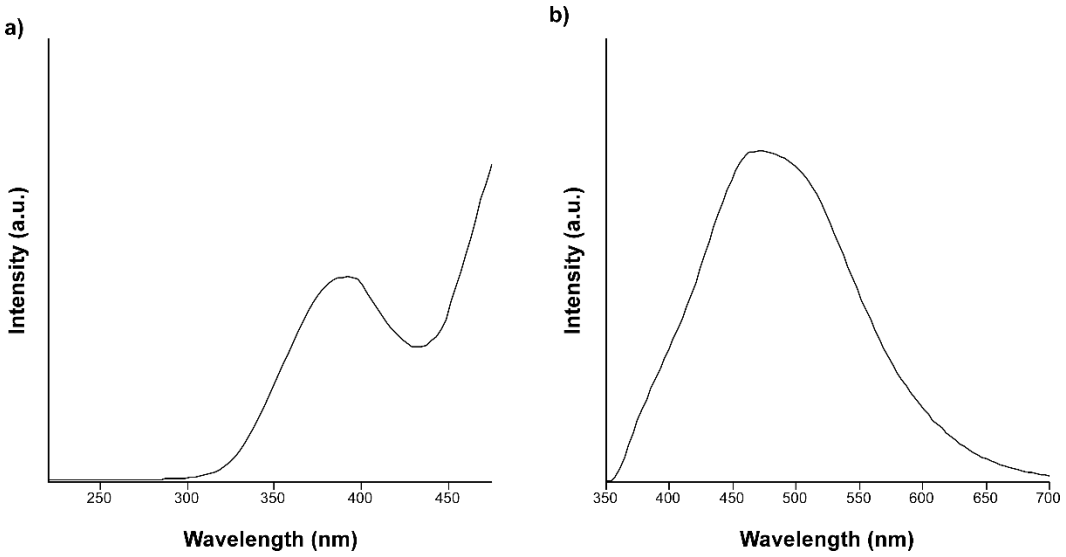

Figure S9. Excitation (λ_{em} = 495 nm) (a) and emission (λ_{em} = 325 nm) (b) spectra of compound **1** recorded at a temperature of 13 K.

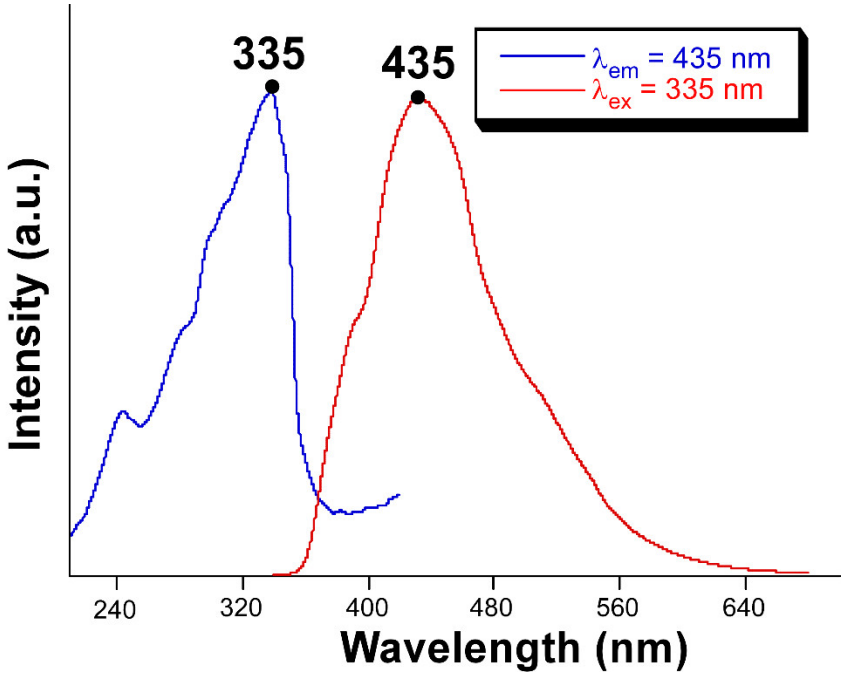

Figure S10. Excitation (λ_{em} = 495 nm) (a) and emission (λ_{em} = 325 nm) (b) spectra of compound **1** recorded at a temperature of 13 K.

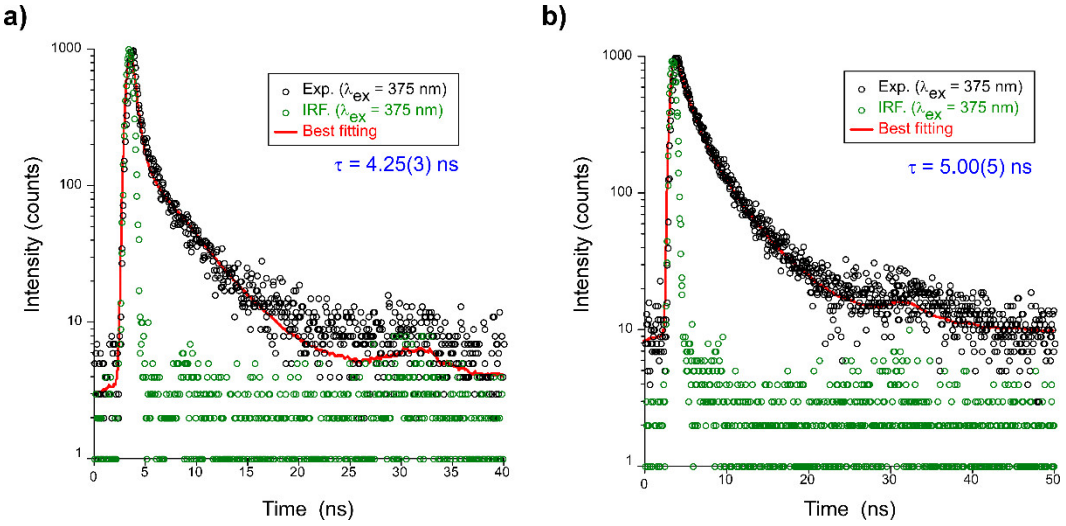

Figure S11. Decay curves of compound **1** recorded at a) room temperature and b) 13 K at an emission wavelength of 495 nm.

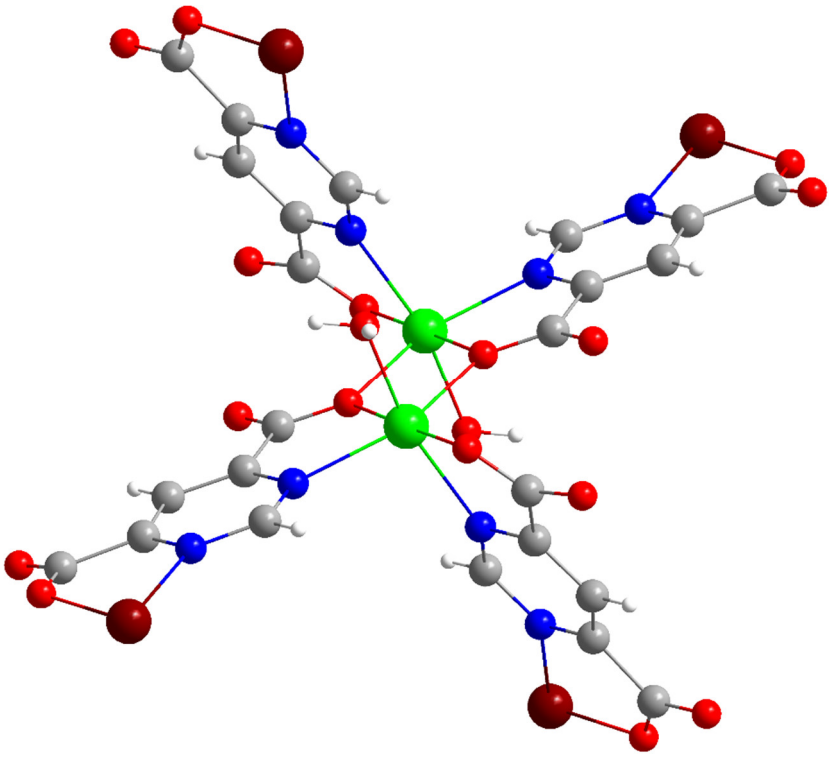

Figure S12. Dimeric model employed for the calculations performed with Gaussian and ORCA programs.

Excitation
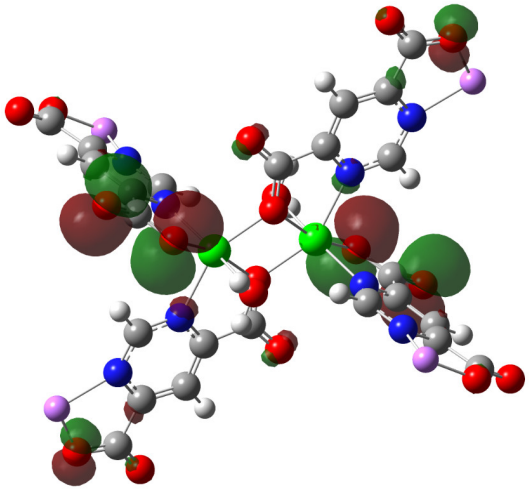
HOMO–15
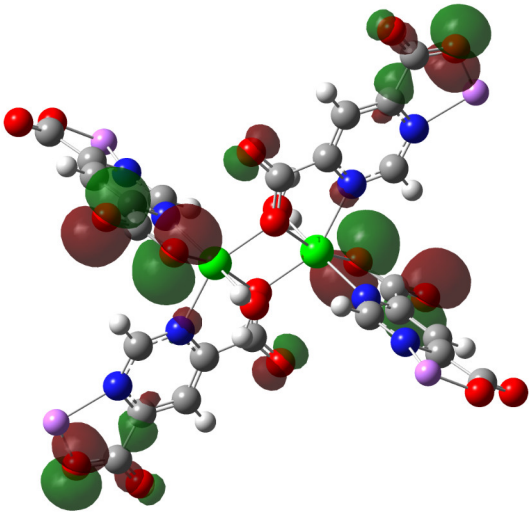
HOMO–14
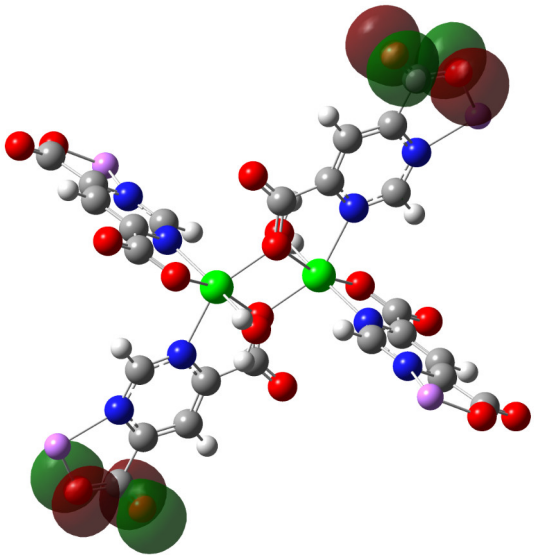
HOMO–11
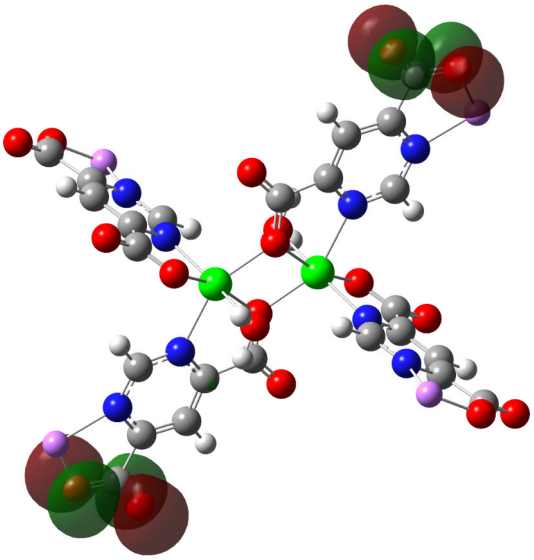
HOMO–10
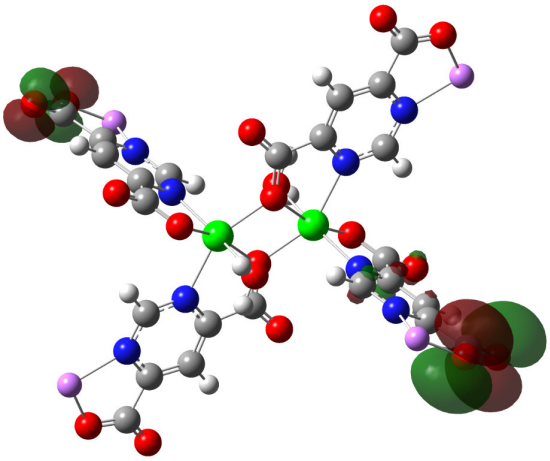
HOMO–7
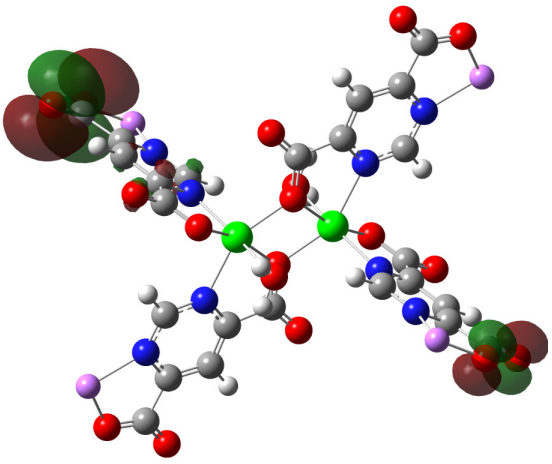
HOMO–6

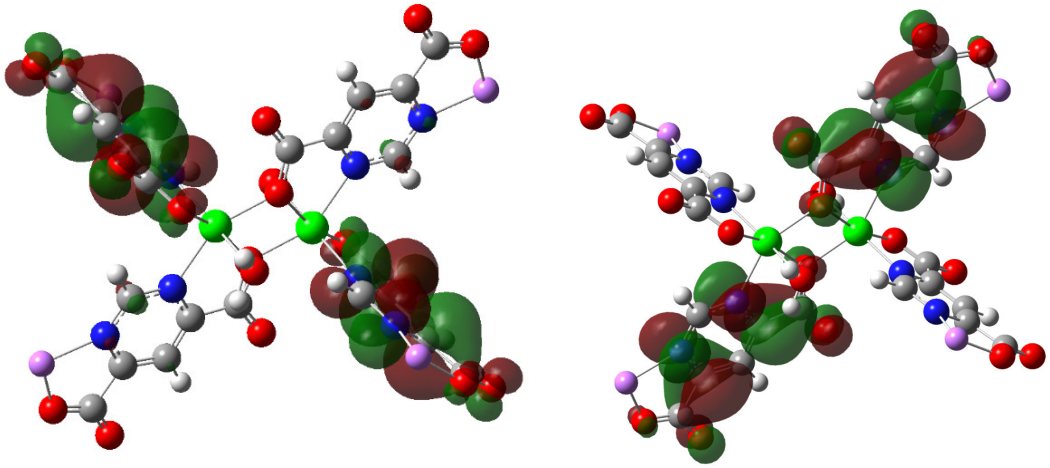

LUMO+3 **LUMO+1**

Emission

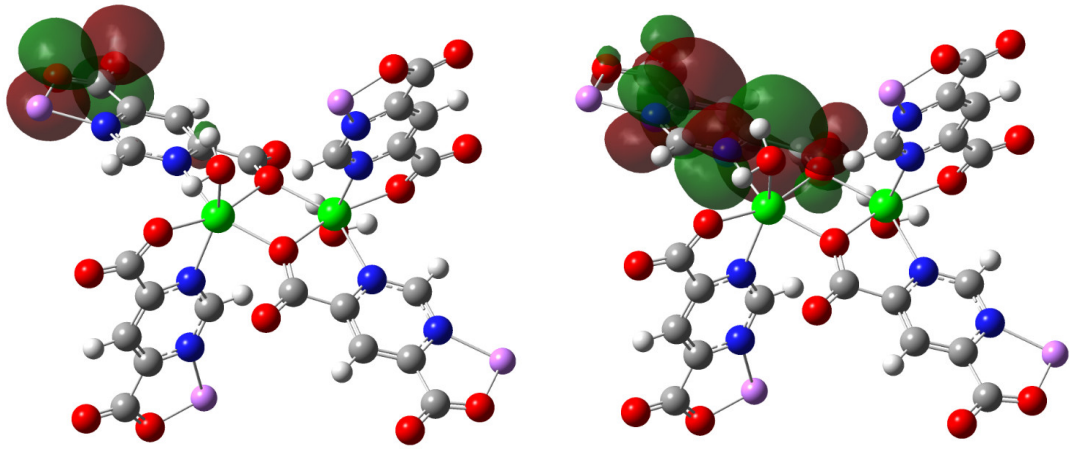

HOMO **LUMO**

Figure S13. MOs of the dimeric model of compound **1** involved in the main excitation and emission.

Table S3. Calculated main excitation and emission energies (nm), singlet electronic transitions and associated oscillator strengths of model 1 in gas phase.

Exp. λ (nm)	Calcd. λ (nm)	Significant contributions	Osc. strength (a.u.)
		Excitation energies	
390	296	HOMO – 15 → LUMO + 3 (42%) HOMO – 14 → LUMO + 2 (45%)	0.0192
390	342	HOMO – 10 → LUMO (78%)	0.0321
390	324	HOMO – 6 → LUMO + 2 (75%)	0.0393
		Emission energies	
495	530	HOMO – 4← LUMO (99%)	0.0282

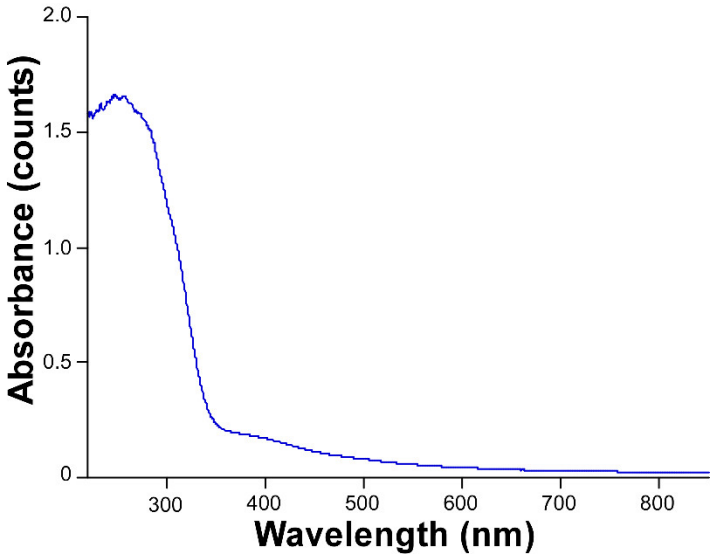

Figure S14. Diffuse reflectance spectrum recorded on polycrystalline sample of compound **1** at room temperature.

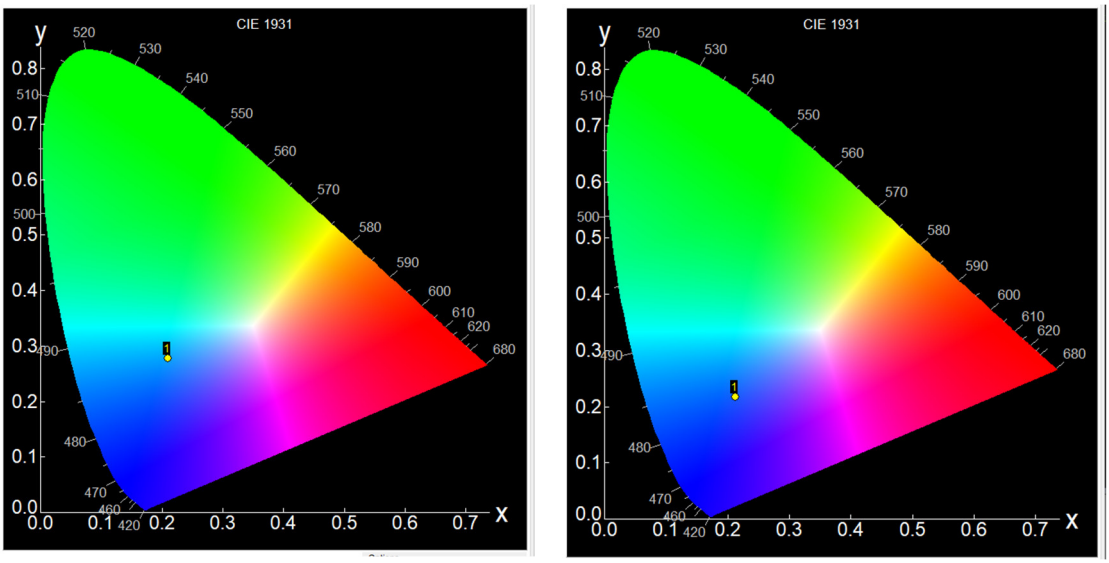

Figure S15. Chromaticity diagrams showing the integrated emission pattern for compound **1** (left) and **1**$_{an}$ (right) at room temperature.

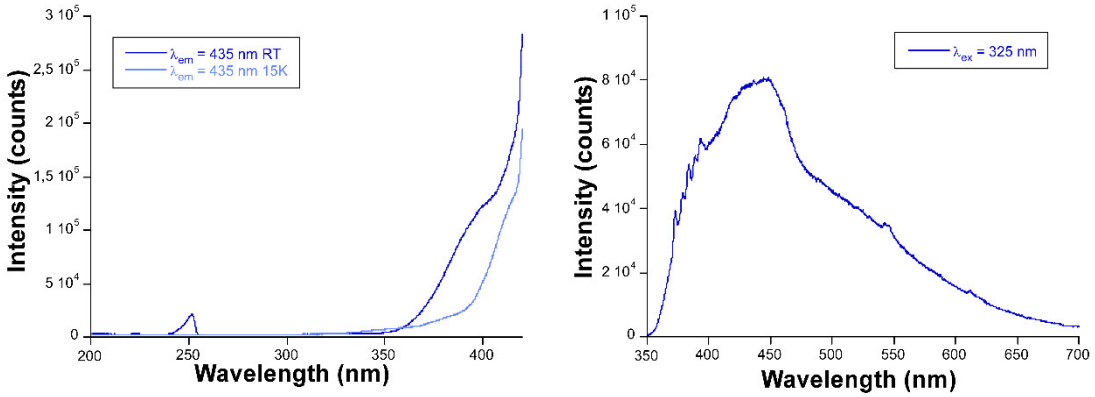

Figure S16. **(a)** Comparative excitation spectra of compound **1**$_{an}$ collected over the main emission line. **(b)** Emission spectrum of **1**$_{an}$ recorded at 15 K.

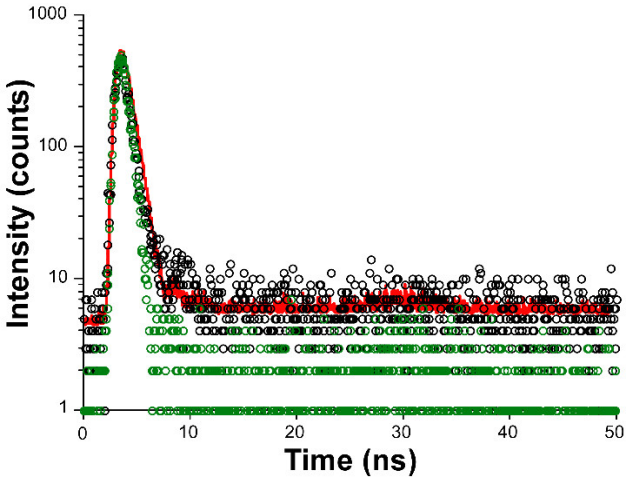

Figure S17. Decay curves of compound **1**$_{an}$ recorded at room temperature at an emission wavelength of 445 nm.